PCCP

PAPER

View Article Online
View Journal | View Issue



Cite this: *Phys. Chem. Chem. Phys.*, 2024, **26**, 6574

# Infrared spectra of $Si_nH_{4n-1}^+$ ions ($n$ = 2–8): inorganic H–(Si–H)$_{n-1}$ hydride wires of penta-coordinated Si in 3c–2e and charge-inverted hydrogen bonds†

Martin Andreas Robert George and Otto Dopfer *

$Si_nH_m^+$ cations are important constituents in silane plasmas and astrochemical environments. Protonated disilane ($Si_2H_7^+$) was shown to have a symmetric three-centre two-electron (3c–2e) Si–H–Si bond that can also be considered as a strong ionic charge-inverted hydrogen bond with polarity $Si^{\delta+}$–$H^{\delta-}$–$Si^{\delta+}$. Herein, we extend our previous work to larger $Si_nH_{4n-1}^+$ cations, formally resulting from adding $SiH_4$ molecules to a $SiH_3^+$ core. Infrared spectra of size-selected $Si_nH_{4n-1}^+$ ions ($n$ = 2–8) produced in a cold $SiH_4/H_2$/He plasma expansion are analysed in the SiH stretch range by complementary dispersion-corrected density functional theory calculations (B3LYP-D3/aug-cc-pVTZ) to reveal their bonding characteristics and cluster growth. The ions with $n$ = 2–4 form a linear inorganic H–(Si–H)$_n$ hydride wire with adjacent Si–H–Si 3c–2e bridges, whose strength decreases with $n$, as evident from their characteristic and strongly IR active SiH stretch fundamentals in the range 1850–2100 cm$^{-1}$. These 3c–2e bonds result from the lowest-energy valence orbitals, and their high stability arises from their delocalization along the whole hydride wire. For $Si_nH_{4n-1}^+$ with $n \geq 5$, the added $SiH_4$ ligands form weak van der Waals bonds to the $Si_4H_{19}^+$ chain. Significantly, because the $Si_nH_{4n-1}^+$ hydride wires are based on penta-coordinated Si atoms leading to supersaturated hydrosilane ions, analogous wires cannot be formed by isovalent carbon.

Received 5th December 2023,
Accepted 30th January 2024

DOI: 10.1039/d3cp05918a

rsc.li/pccp



## Introduction

Hydrogen passivation converts reactive $Si_n$ clusters into stable polysilanes nanostructures ($Si_nH_m$), with potential applications of their derivatives and ions in material science, inorganic chemistry, catalysis, plasma- and astrochemistry, and theoretical chemistry.[1–25] For example, polysilane oligomers and their radical ions reveal interesting electronic, photophysical, and optical properties arising from substantial $\sigma$-delocalization of the bonding Si–Si electrons.[1,26] Recently, higher-order silanes have been identified during monosilane pyrolysis by gas chromatography–mass spectrometry.[21] From an astrochemical point of view, Si and H are amongst the ten most abundant elements in the universe, and thus $Si_nH_m$ molecules and their ions are expected to occur in the interstellar medium, although so far only $SiH_4$ has been identified.[22] In the laboratory, saturated $Si_nH_{2n+2}$ polysilanes up to $n$ = 19 have been produced from bombarding $SiH_4$ ices with electrons and detected by mass spectrometry.[27] The discussed production mechanism involves radical–radical recombination and insertion reactions, although their structures have remained elusive. The structure and reactivity of $Si_nH_m^+$ cations relevant for silane plasmas used in plasma-enhanced chemical vapor deposition for the industrial fabrication of Si-based microelectronic thin films and devices[17–20] have mostly been characterized by mass spectrometry.[15,16,28,29] However, firm identification of structure and bonding of $Si_nH_m^+$ ions in plasma and astrochemical environments requires spectroscopic characterization, which is still rather scarce for ions with $n \geq 2$.[30–33] In the condensed phase, silyl cations are highly reactive,[8,11] and only recently a $SiH_3^+$ compound could be synthesized and characterized.[14]

Although Si and C are both group IV elements, their bonding properties differ substantially,[34] which partly arises from their different electronegativity with respect to H (EN = 1.90, 2.20, 2.55 for Si, H, C on the Pauling scale). Due to their weaker and less directional Si–Si and Si–H bonds, $Si_nH_m$ molecules exhibit a larger variety of bonding motifs as compared to the corresponding $C_nH_m$ molecules. For example, different from $C_nH_m$, $Si_nH_m$ have more frequently Si–H–Si bridges, characterized by a three-center two-electron (3c–2e) bond.[35,36] In amorphous and crystalline silicon ($a$-Si:H and $c$-Si), used for example in commercial solar cells, linear Si–H–Si bridges are typical binding

*Institut für Optik und Atomare Physik, Technische Universität Berlin, Hardenbergstr. 36, Berlin 10623, Germany. E-mail: dopfer@physik.tu-berlin.de*

† Electronic supplementary information (ESI) available. See DOI: https://doi.org/10.1039/d3cp05918a

motifs for proton impurities. In *c*-Si, they form well-defined linear and symmetric Si–H–Si bonds.[37] The Si–H–Si 3c–2e bond was first detected in crystals of cyclic and linear silyl cations.[38–40] Subsequently, infrared photodissociation (IRPD) spectroscopy has been used in our group to characterize such 3c–2e bonds in a variety of $Si_nH_m^+$ cations in the gas phase, *i.e.* free from any perturbation by matrix effects and counter ions. The studied ions include protonated disilane ($Si_2H_7^+$),[31] an isomer of trisilane ($Si_3H_8^+$),[32] and $Si_nH_{4n-4}^+$ ions ($n$ = 4–8)[33] which may formally be described as silane aducts of the unsaturated sylilene cation, $Si_2H_4^+(SiH_4)_{n-2}$. The characteristic IR fingerprint of the Si–H–Si bond is its strongly IR active antisymmetric stretch fundamental ($\sigma_{SiHSi}$) occurring in the 1600–2100 $cm^{-1}$ range, whose frequency strongly depends on the structural and energetic details of the Si–H–Si bridges.[33] The strength of the Si–H–Si bonds can range from strong 3c–2e chemical bonds to very weak van der Waals contacts (5–150 kJ $mol^{-1}$).[33] In the covalent case, the molecular orbital describing the 3c–2e bond is the lowest-energy valence orbital, illustrating its high stability.[31,32] Because the EN of H is higher than that of Si, these 3c–2e bonds can also be considered as strong ionic charge-inverted hydrogen bonds (CIHB),[41,42] with polarity $Si^{\delta+}$–$H^{\delta-}$–$Si^{\delta+}$ resulting in the limit of ionic bonding in a hydride ($H^-$) bond. This is opposite to regular $A^{\delta-}$–$H^{\delta+}$–$B^{\delta-}$ hydrogen bonds (H-bonds) in which, according to the IUPAC definition,[43] a positive H atom (proton) is located between two basic atoms A (proton donor) and B (proton acceptor) with higher EN.

Herein, we extend our previous IRPD studies on silane cations to the $Si_nH_{4n-1}^+$ series with $n$ = 2–8 to probe their structure, bonding and cluster growth mechanism as a function of the cluster size, along with complementary calculations. The most stable structures of these supersaturated hydrosilane ions may formally be considered as $SiH_3^+(SiH_4)_{n-1}$ clusters and exhibit unprecedented inorganic silicon hydride wires, H–(Si–H)$_n$ with multiple 3c–2e Si–H–Si bonds of penta-coordinated Si atoms. These 3c–2e bonds get weaker as the chain grows and, starting from $n$ = 5, the $Si_4H_{15}^+$ wire is solvated by $SiH_4$ ligands *via* weak van der Waals bonds. The $Si_nH_{4n-1}^+$ ions differ qualitatively from the previously studied $Si_nH_{4n-4}^+$ series[33] because they do not contain any Si–Si and/or Si=Si bonds. While $SiH_3^+$ and $Si_2H_7^+$ ($n$ = 1 and 2) have been well studied by IR spectroscopy,[31,44–46] mass spectrometry,[15,31,47,48] and calculations,[31,49,50] the only study available for $n \geq 3$ utilizes high-pressure mass spectrometry to determine the binding enthalpies of $SiH_3^+(SiH_4)_{n-1}$ as $-\Delta H_0$ = >146, 37.7, and 13.8 kJ $mol^{-1}$ for $n$ = 2–4, respectively.[15] Although these data are not sensitive to structure, the authors concluded symmetric bonding of two $SiH_4$ ligands to the two sides of the $3p_z$ orbital of the planar $SiH_3^+$ cation and thus closure of the first solvation shell at $n$ = 3.

## Results and discussion

IRPD spectra of size-selected $Si_nH_{4n-1}^+$ ions with $n$ = 2–8 in the SiH stretch range (1400–2300 $cm^{-1}$, Fig. 1, Table 1) were obtained in a tandem quadrupole mass spectrometer coupled to an electron ionization source.[51,52] The ions were produced in a pulsed supersonic plasma expansion of a $SiH_4/H_2$/He gas mixture (ratio 1/1/38) at 3 bar stagnation pressure. This setup was used previously to record IRPD spectra of bare $Si_nH_{4n-4}^+$ ions and Ar/Ne tagged $Si_2H_6^+$,[30] $Si_3H_8^+$,[32] $SiH_3OH_2^+$,[53] and $Si_2H_7^+$.[31] Chemical ionisation of this gas mixture causes silane polymerization reactions forming $Si_nH_{4n-1}^+$ up to $n$ = 8. They form in barrierless aggregation reactions of $SiH_4$ units to $SiH_3^+$,[15,31,32] which is the major fragment of ionizing $SiH_4$. A typical mass spectrum of the ion source is shown in Fig. S1 in the ESI.† $Si_nH_{4n-1}^+$ ions selected by the first quadrupole were irradiated with a tuneable IR laser pulse of an optical parametric oscillator ($\nu_{IR}$, 2–5 mJ, 10 Hz repetition rate, 1 $cm^{-1}$ bandwidth). Resonant vibrational excitation by single-photon absorption resulted in the evaporation of either one ($n$ = 3–4) or

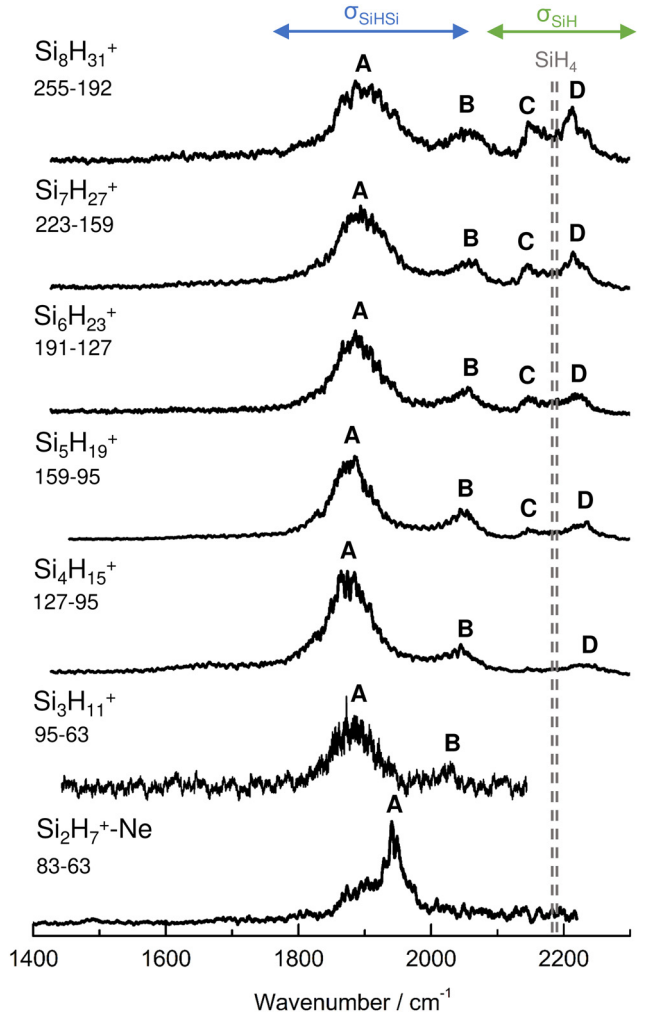


Fig. 1 IRPD spectra of $Si_nH_{4n-1}^+$ ($n$ = 3–8) in the SiH stretch range recorded in the $SiH_4$ or $2SiH_4$ loss channel as indicated by the $m/z$ values of parent and daughter ions. The $Si_2H_7^+$Ne spectrum ($n$ = 2) recorded in the Ne loss channel is included for comparison.[31] The probed spectral range (1400–2300 $cm^{-1}$) covers $\sigma_{SiH}$ fundamentals (**C**/**D**) of free Si–H bonds and $\sigma_{SiHSi}$ modes (**A**/**B**) of 3c–2e bonds (Table 1). The dashed lines indicate the positions of the SiH stretch modes of bare $SiH_4$ at $\nu_1(a_1)$ = 2187 and $\nu_3(t_2)$ = 2191 $cm^{-1}$.[54]

Table 1 Positions and widths (fwhm in parenthesis) in $cm^{-1}$ of the transitions observed in the IRPD spectra of $Si_nH_{4n-1}^+$ (Fig. 1) compared to frequencies of $SiH_4$

| Peak | Mode | $SiH_4$[a] | $Si_2H_7^+Ne$[b] | $Si_3H_{11}^+$ | $Si_4H_{15}^+$ | $Si_5H_{19}^+$ | $Si_6H_{23}^+$ | $Si_7H_{27}^+$ | $Si_8H_{31}^+$ |
|---|---|---|---|---|---|---|---|---|---|
| **A** | $\sigma_{SiHSi(a)}$ | | 1941 (30) | 1886 (65) | 1873 (70) | 1877 (65) | 1885 (70) | 1893 (80) | 1903 (100) |
| **B** | $\sigma_{SiHSi(s)}$ | | | 2031 (15) | 2045 (50) | 2051 (45) | 2055 (60) | 2058 (60) | 2060 (60) |
| **C** | $\sigma_{SiH}$ | 2187 | | | | 2144 (25) | 2147 (30) | 2144 (25) | 2147 (35) |
| **D** | $\sigma_{SiH}$ | 2191 | | | 2236 (45) | 2235 (40) | 2225 (40) | 2216 (40) | 2211 (45) |

[a] Ref. 54. [b] Ref. 31.



two ($n \geq 5$) $SiH_4$ molecules, indicating a formal cluster composition of $SiH_3^+(SiH_4)_{n-1}$ with decreasing $SiH_4$ binding energy as $n$ increases. IRPD spectra were then obtained as a function of $\nu_{IR}$ by monitoring the fragment ions selected by the second quadrupole and normalization for laser intensity. Because the $SiH_4$ binding energy of $Si_2H_7^+$ (*ca.* 150 kJ $mol^{-1}$) is much higher than the employed IR photon energy (<25 kJ $mol^{-1}$), its spectrum could only be obtained by Ne/Ar tagging.[31] This spectrum was reported and analysed previously[31] and is included in Fig. 1 only for comparison.

The four major peaks **A–D** observed in the IRPD spectra are readily assigned to the strongly IR active Si–H–Si stretch modes of the 3c–2e bond(s) between 1800 and 2100 $cm^{-1}$ ($\sigma_{SiHSi}$, **A** and **B**) and the much weaker SiH stretch modes of the free Si–H bonds between 2100 and 2300 $cm^{-1}$ ($\sigma_{SiH}$, **C** and **D**). For comparison, Fig. 1 also indicates the symmetric and triply degenerate antisymmetric SiH stretch frequencies of bare $SiH_4$ by dashed lines, $\nu_1(a_1)/\nu_3(t_2)$ = 2187/2191 $cm^{-1}$.[54] Significantly, while $\nu_1$ is IR forbidden in bare $SiH_4$, it becomes slightly allowed by the presence of the nearby positive charge and experiences shifts and splittings. The IRPD spectra are dominated by peak **A**, assigned to antisymmetric $\sigma_{SiHSi(a)}$ modes of the Si–H–Si 3c–2e bonds by comparison to the previous analysis of the $Si_2H_7^+$ and $Si_nH_{4n-4}^+$ spectra. This band experiences a substantial monotonic red shift from 1941 to 1873 $cm^{-1}$ for $n$ = 2–4 (by −55 to −13 $cm^{-1}$), while it shows smaller incremental blue shifts of +4, +8, +8, and +10 $cm^{-1}$ for $n$ = 5–8, indicating a change in bonding at $n$ = 5. Starting from $n$ = 3, band **B** assigned to the corresponding symmetric $\sigma_{SiHSi(s)}$ modes of the 3c–2e bonds grow in intensity. This mode exists only for $n \geq 3$, indicating the appearance of a second Si–H–Si 3c–2e bond in $Si_3H_{11}^+$. Band **B** experiences gradual monotonic blue shifts by +14, +6, +4, +3, and +2 $cm^{-1}$ for $n$ = 4–8. The magnitude of the shifts drops for $n \geq 5$, again indicating a change in bonding in this size regime. Bands **C** and **D** occur in the range of the free SiH stretch modes and grow roughly linearly in intensity starting from $n$ = 5, again indicating a change in bonding at this size range. Their positions at around 2145 and 2225 $cm^{-1}$ hardly change as a function of $n$, although their widths get somewhat broader. Hence, the first rough analysis of the number and position of the IRPD bands, and their incremental shifts and changes in IR activity suggests a $Si_nH_{4n-1}^+$ cluster growth with the formation of chemical 3c–2e bonds up to $n$ = 4 and subsequent attachment of weakly bonded $SiH_4$ ligands attached to a $Si_4H_{15}^+$ core ion by induction and dispersion forces. The weaker $SiH_4$ binding energy of the larger ions is also visible in the photofragmentation branching ratios measured at band **A** (Table S1 in the ESI†). While $Si_nH_{4n-1}^+$ ions with $n \leq 4$ evaporate only one $SiH_4$ ligand, those with $n \geq 5$ can dissociate two ligands at an IR photon energy of around 2000 $cm^{-1}$. Neglecting kinetic energy release and assuming that the absorbed photon energy is merely used for ligand dissociation (and not for changes in internal energy) and all $SiH_4$ ligands have the same binding energy for $n$ = 5–8, one can bracket their dissociation energy as $D_0$ = 850 ± 150 $cm^{-1}$ or 10.2 ± 1.8 kJ $mol^{-1}$. This value is consistent with the $SiH_4$ binding enthalpy of the somewhat stronger bonded $n$ = 4 ion reported as $-\Delta H_0$ = 13.8 ± 1.3 kJ $mol^{-1}$.[15]

For a more detailed structural and vibrational assignment and the analysis of chemical bonding (charge distributions, binding energies, molecular orbitals), quantum chemical calculations were performed at the dispersion-corrected B3LYP-D3/aug-cc-pVTZ level for $Si_nH_{4n-1}^+$ ions with $n \leq 5$ (Fig. 2, Fig. S2–S7 and Tables S2–S5 in ESI†). Reported relative energies ($E_0$) and binding energies ($D_0$) are corrected for harmonic zero-point vibrational energies. All calculated frequencies are scaled by a factor of 0.97878 to optimize the agreement between the calculated and measured $\nu_{SiH}$ frequencies of $SiH_3$ and $SiH_4$. The atomic charge distribution is evaluated using the natural bond orbital (NBO) analysis. We consider herein mainly the most stable structure for each cluster size, while information for less stable local minima is provided in the ESI.†

Our calculations yield a planar structure for $SiH_3^+$ ($D_{3h}$) with a Si–H bond length and stretch frequencies ($r_e$ = 1.470 Å, $\nu_{1/3}$ = 2218/2295 $cm^{-1}$) in good agreement with previous experimental and computational data.[55,56] In line with the EN of Si and H, the partial charges are $q_H$ = −124 and $q_{Si}$ = +1371 me. The closed-shell $SiH_3^+$ cation ($^1A_1$) has a vacant and thus rather electrophilic $3p_z$ orbital, which serves as attractive binding sites for neutral ligands, such as rare gas atoms,[57] $H_2$,[45,46] or $H_2O$.[53] Barrierless attachment of $SiH_4$ to this orbital results in protonated disilane, $Si_2H_7^+$, forming a strong symmetric Si–H–Si 3c–2e bond characterized in detail previously.[31] Our computed binding energy for $SiH_4$ loss ($D_0$ = 150.1 kJ $mol^{-1}$) agrees well with the measured bond enthalpy ($-\Delta H_0$ > 146 kJ $mol^{-1}$)[15] and our previous MP2 and CBS-QB3 calculations (148.2 and 150.1 kJ $mol^{-1}$).[31] The $SiH_4$ ligand attacks the $3p_z$ orbital with one of the negative H atoms of $SiH_4$ ($q_H$ = −161 and $q_{Si}$ = +643 me) in a bent configuration with $C_2$ symmetry ($\theta$ = 144°), which is slightly more stable than the linear Si–H–Si structure ($D_{3h/3d}$) by only a few kJ $mol^{-1}$ (<5 kJ $mol^{-1}$),[31] indicating a rather flat and anharmonic double minimum potential for

 

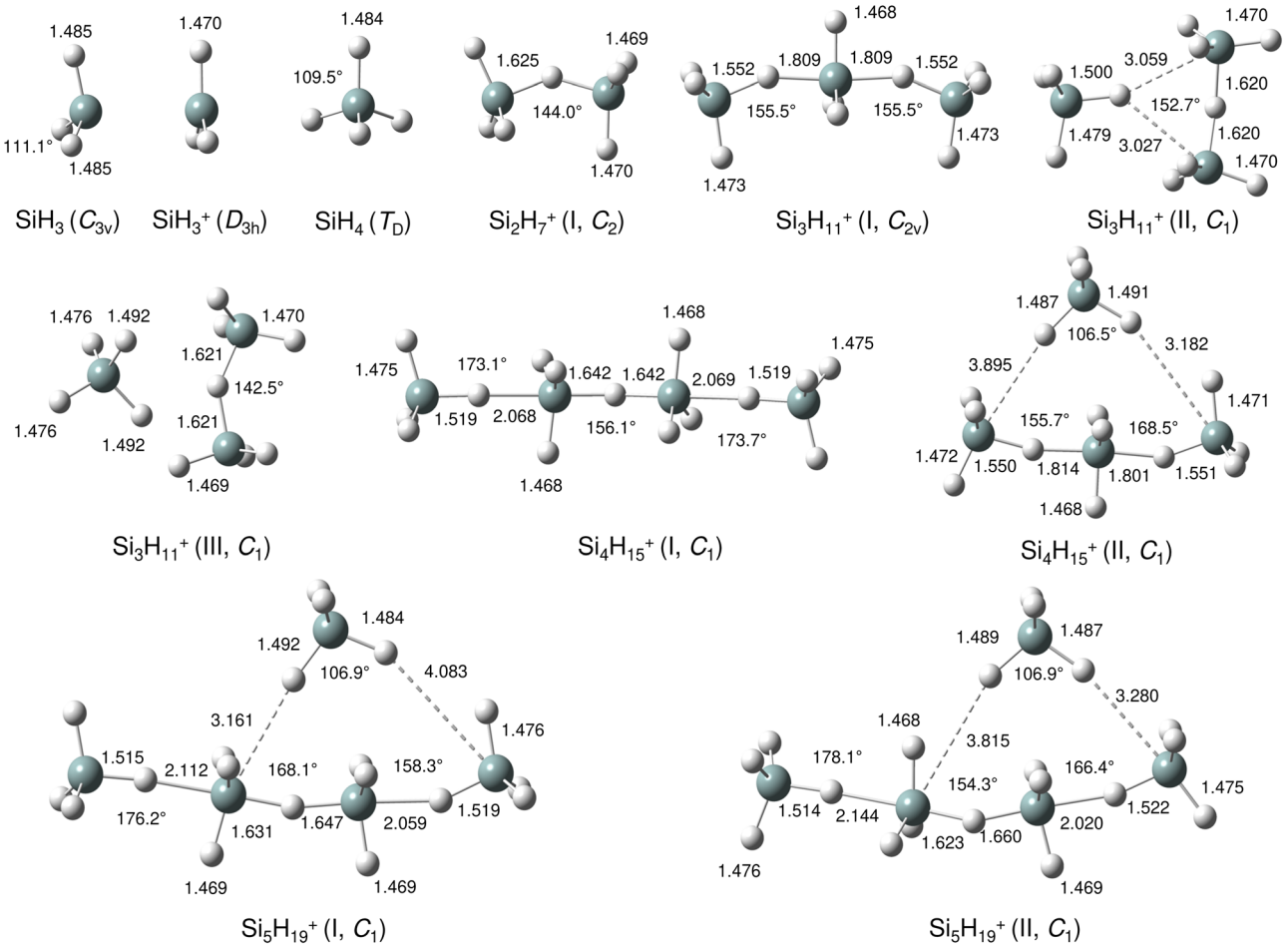


Fig. 2 Lowest energy structures of $SiH_3$, $SiH_3^+$, $SiH_4$, $Si_2H_7^+$, $Si_3H_{11}^+$(I–III), $Si_4H_{15}^+$(I,II) and $Si_5H_{19}^+$(I,II) in their ground electronic states calculated at the B3LYP-D3/aug-cc-pVTZ level. Selected bond lengths and bond angles are given in Å and degree, respectively.

H motion perpendicular to the Si–Si axis. The $SiH_3$ groups become slightly nonplanar (intermediate between $sp^2$ and $sp^3$ hybridisation) and the barriers for hindered internal rotation are rather low (<3 kJ mol$^{-1}$).[31] The corresponding molecular orbital (MO) describing the rather strong 3c–2e bond (1.625 Å) is delocalized along the Si–H–Si bridge and is the lowest valence MO (HOMO-6, Fig. 3). Although formally a proton is added to $Si_2H_6$, the bridging H atom has a negative charge of $q_H = -304$ me, while the two Si atoms carry most of the excess positive charge ($q_{Si} = +954$ me), and are thus attractive binding sites for both rare gas[31] and further $SiH_4$ ligands. The alternating charge distribution in $Si^{\delta+}$–$H^{\delta-}$–$Si^{\delta+}$ qualifies $Si_2H_7^+$ as prototypical cationic example of a CIHB, and its formation causes charge transfer of 348 me from $SiH_3^+$ to $SiH_4$. The strongly IR active antisymmetric SiH stretch mode is computed as $\sigma_{SiHSi} = 1975$ cm$^{-1}$ ($I = 1314$ km mol$^{-1}$), in good agreement with the value of the Ne-tagged complex (1941 cm$^{-1}$).

By far, the most stable structure of $Si_3H_{11}^+$ is obtained by barrierless attachment of $SiH_4$ to a Si atom of $Si_2H_7^+$ (isomer I, Fig. 2). In this $C_2$ symmetric structure, two equivalent $SiH_4$ ligands bind to the $3p_z$ orbital of a central $SiH_3^+$ cation forming two strongly asymmetric and bent 3c–2e bonds (1.809 and 1.552 Å, 155.5°). According to the much longer Si–H bond in the bridge (1.809 *vs.* 1.625 Å), the $SiH_4$ binding energy is computed to be much weaker than in $Si_2H_7^+$ (40.8 *vs.* 150.0 kJ mol$^{-1}$) but again in excellent agreement with the measured bond enthalpy of $-\Delta H_0 = 37.7 \pm 1.3$ kJ mol$^{-1}$.[15] The lower binding energy enables the IRPD spectrum of $Si_3H_{11}^+$ to be recorded without tagging. This $S_N2$ like complex features one penta-coordinated Si atom and can be considered as a supersaturated hydrosilane molecule, because even protonated aliphatic trisilane would only have nine H atoms for three Si atoms ($Si_3H_9^+$). Formation of the two CIHBs causes charge transfer of 433 me from $SiH_3^+$ to the two $SiH_4$ ligands. The two negative H atoms in $Si_3H_{11}^+$ carry a slightly more negative charge than in $Si_2H_7^+$ (−306 *vs.* −304 me). The two MOs describing the two 3c–2e bonds are completely delocalized along the Si–H–Si–H–Si bridge and are again the two lowest valence MOs (HOMO-9/10, Fig. 3). The coupling of the two $\sigma_{SiHSi}$ modes of the two 3c–2e bonds results in a splitting of the $\sigma_{SiHSi}$ mode of 1975 cm$^{-1}$ of $n = 2$ in a rather weak symmetric and a rather strong antisymmetric normal mode at $\sigma_{SiHSi(s)}$ = 2031 cm$^{-1}$ and $\sigma_{SiHSi(a)}$ = 1904 cm$^{-1}$ for $n = 3$, respectively. These bands are in excellent agreement with the observed

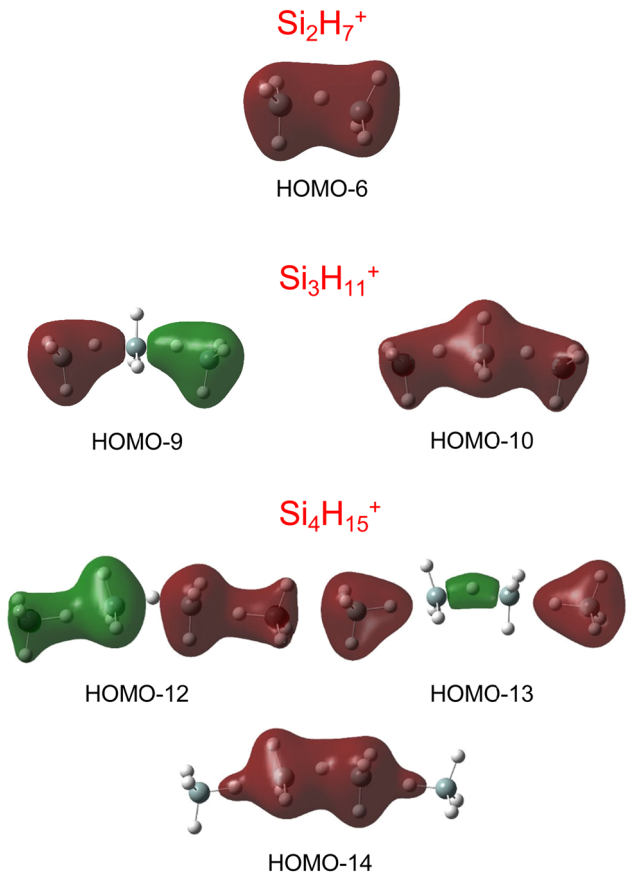


Fig. 3 Visualisation of the lowest valence MOs of the most stable structures of $Si_2H_7^+$, $Si_3H_{11}^+$, and $Si_4H_{15}^+$, representing the 3c–2e bonds.

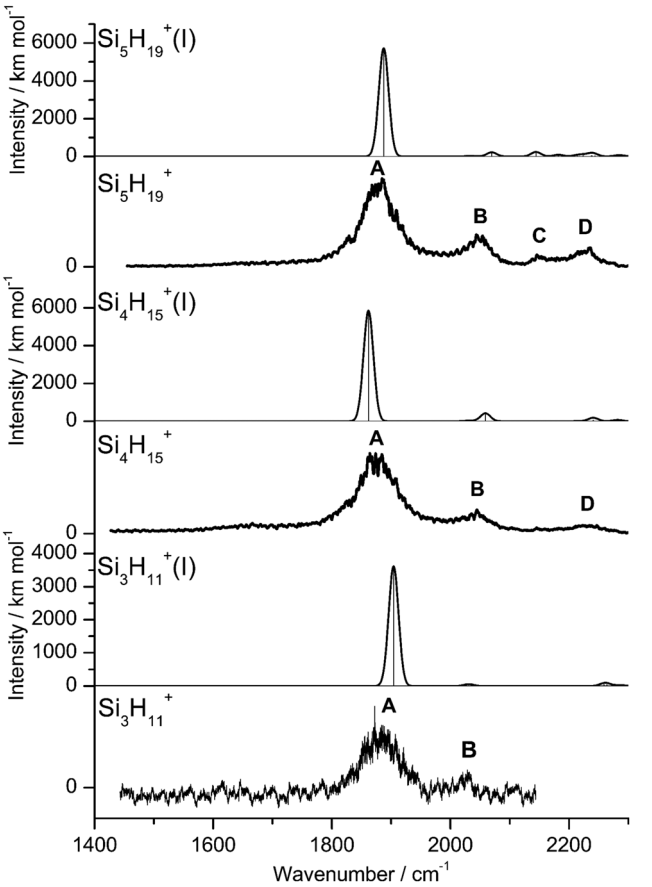


Fig. 4 Experimental IRPD spectra of $Si_3H_{11}^+$, $Si_4H_{15}^+$, and $Si_5H_{19}^+$ compared to linear IR absorption spectra of the most stable isomers calculated at the B3LYP-D3/aug-cc-pVTZ level (Table S2 in ESI†).

bands **B** and **A** predicted at 2031 and 1886 cm$^{-1}$ with respect to their absolute frequency, the frequency shifts with respect to band **A** of $Si_2H_7^+$, and their relative IR activities (Fig. 4). We also calculated two further less stable $Si_3H_{11}^+$ isomers (II and III), in which $SiH_4$ ligands are attached to the side of a $Si_2H_7^+$ core ion by much weaker induction and dispersion forces ($D_0$ = 13.8 and 12.3 kJ mol$^{-1}$) and these feature only one 3c–2e bond. As a consequence, their predicted IR spectra are rather similar to that of $Si_2H_7^+$ and in strong contradiction with the experiment (Fig. S3 in ESI†). Hence, we do not discuss them further here.

The most stable structure of $Si_4H_{15}^+$ (isomer I) is derived by barrierless addition of a further $SiH_4$ ligand to a terminal Si atom of the linear $Si_3H_{11}^+$ wire. In this nearly symmetric structure, two almost equivalent $SiH_4$ ligands bind to the highly positive Si atoms of a central $Si_2H_7^+$ cation forming a rather strong symmetric 3c–2e bond in the middle of the wire (1.642 Å, 156°) and two nearly equivalent and weaker asymmetric 3c–2e bonds at both ends (2.069 and 1.519 Å, 173°). (The $C_2$ symmetric structure is predicted as a transition state.) The MOs describing the three 3c–2e bonds are again completely delocalized along the Si–H–Si–H–Si bridge and these are again the three lowest valence MOs (HOMO-12/13/14, Fig. 3). The binding energy of the terminal $SiH_4$ units drops further down to $D_0$ = 14.6 kJ mol$^{-1}$, again in excellent agreement with the measured bond enthalpy of $-\Delta H_0$ = 13.8 ± 1.3 kJ mol$^{-1}$.[15] The lower binding energy is consistent with the smaller charge transfer from $Si_3H_{11}^+$ to the added $SiH_4$ ligand (110 me). This linear inorganic hydride wire features two penta-coordinated Si atoms and is an even more supersaturated silane molecule than $Si_3H_{11}^+$, because protonated aliphatic tetrasilane has eleven H atoms for four Si atoms ($Si_4H_{11}^+$), *i.e.* four H atoms less than $Si_4H_{15}^+$. Attachment of the two $SiH_4$ ligands at opposite ends of $Si_2H_7^+$ changes its parameters with respect to both bond lengths and angle of the 3c–2e bridge (1.642 Å and 156° *vs.* 1.625 Å and 144°) and the negative charge on the central H atom ($q_H$ = −317 *vs.* −304 me). The three 3c–2e bonds have their characteristic $\sigma_{SiHSi}$ modes predicted at 1862 (very strong), 2032 (very weak), and 2059 (weak) cm$^{-1}$, with $I$ = 5844, 34, and 423 km mol$^{-1}$, respectively. These predicted frequencies show again good agreement with the corresponding bands **A** and **B** at 1873 and 2045 cm$^{-1}$, where the latter band covers both weak $\sigma_{SiHSi}$ modes (Fig. 4). Finally, the weak band **D** at 2236 cm$^{-1}$ can also be explained by unresolved $\sigma_{SiH}$ modes with low IR activity in this spectral range. We also computed further less stable $Si_4H_{15}^+$ isomers, in which either one $SiH_4$ ligand is attached to the side of $Si_3H_{11}^+$ or two $SiH_4$ ligands attached to the side of $Si_2H_7^+$, all with $D_0$ < 12 kJ mol$^{-1}$. As their predicted IR spectra do not match the

 

measured IRPD spectrum recorded for $Si_4H_{15}^+$, they are not considered further here (Fig. S4 in ESI†).

For the $Si_5H_{19}^+$ ions, our calculations yield six low-energy isomers, all within an energy range of 4 kJ mol$^{-1}$. The binding energy for adding $SiH_4$ ligands to the $Si_nH_{4n-1}^+$ wire drops with the length of the chain, and at $n = 5$ it is no longer favourable to extend the $Si_4H_{15}^+$ chain further in a linear fashion. Indeed, we could not find a stable minimum for such a $n = 5$ chain, because the added $SiH_4$ ligand prefers to move closer to the central $Si_2H_7^+$ unit, which carries a substantial amount of the positive excess charge. To this end, the global minimum identified for $Si_5H_{19}^+$ has a $SiH_4$ unit attached to the side of the $Si_4H_{15}^+$ wire, with $D_0 = 10.6$ kJ mol$^{-1}$ and very long SiH$\cdots$Si contacts (3.161 and 4.083 Å). Further low-energy minima can be obtained for other isomers, with one $SiH_4$ attached to $Si_4H_{15}^+$ or two $SiH_4$ ligands attached to the $Si_3H_{11}^+$ core *via* induction and dispersion forces. The IR spectra predicted for $Si_5H_{19}^+$ clusters with one or two $SiH_4$ ligands are quite different, because the core ions, $Si_4H_{15}^+$ or $Si_3H_{11}^+$, determine the coarse structure in the strongly IR active $\sigma_{SiHSi}$ range. Comparison of these spectra with the measured IRPD spectrum suggests that the core in the observed $Si_5H_{19}^+$ ions is the $Si_4H_{15}^+$ wire. Depending on the exact position of the last weakly-bonded $SiH_4$ ligand in $Si_5H_{19}^+$, the symmetry, structure, charge distribution, and IR spectrum changes slightly. Taking the computed global minimum, the charge transfer from $Si_4H_{15}^+$ to $SiH_4$ is rather small (7 me). The intense $\sigma_{SiHSi}$ transition predicted at 1887 cm$^{-1}$ agrees well with band **A** observed at 1877 cm$^{-1}$, while the two lower-intensity $\sigma_{SiHSi}$ modes computed at 2033 and 2070 cm$^{-1}$ match with peak **B** at 2051 cm$^{-1}$. In the higher frequency range, the $\sigma_{SiH}$ modes of the $SiH_4$ ligand and $SiH_3$ units predicted at 2144, 2182, 2214, 2224, 2238, 2239, and 2244 cm$^{-1}$ can be attributed to the weak broad and unresolved peaks **C** and **D** at 2144 and 2235 cm$^{-1}$, respectively.

No calculations have been performed for $Si_nH_{4n-1}^+$ clusters with $n \geq 6$, because of their multiple low-energy local minima, which differ from their global minimum merely by the different attachment of weakly-bonded $SiH_4$ ligands to the linear $Si_4H_{15}^+$ core. The excellent agreement of the measured $\sigma_{SiHSi}$ frequencies with those calculated for the global minima obtained for $n \leq 5$ in Fig. 4 confirms the deduced cluster growth. The intense band **A** drops significantly in frequency for $n = 2$–4 and increases the monotonically for $n \geq 4$ with a smaller slope, confirming the change in bonding mechanism from chemical to van der Waals between $n = 4$ and 5 (Fig. 5).

In the following, we analyse the binding properties in the identified H–(Si–H)$_n$ wire in more detail. In general, Si–H–Si bridges are often formed by a 3c–2e bond in which two electrons in a bonding orbital establish two stable chemical bonds. These Si–H$\cdots$Si H-bonds in $Si_nH_m^+$ cations feature a cationic CIHB, because the EN of Si is lower than that of H, leading to a charge configuration ($Si^{\delta+}$–$H^{\delta-}\cdots Si^{\delta+}$) opposite from that of a conventional $\sigma$-type H-bond between a proton donor A and an acceptor B ($A^{\delta-}$–$H^{\delta+}\cdots B^{\delta-}$). However, in many aspects these CIHBs show similar features as the regular H-bonds, including the redshifts of the proton donor stretch

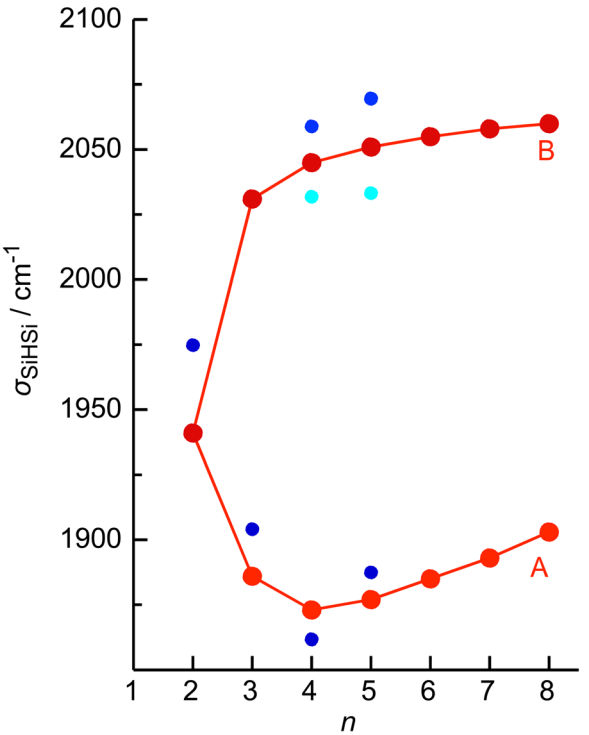


Fig. 5 Experimental $\sigma_{SiHSi}$ frequencies of $Si_nH_{4n-1}^+$ (bands A and B, red) as a function of $n$ compared to computed values for the strongest (blue) and weaker (cyan) component, illustrating the change from strong chemical to weak van der Waals bonding between $n = 4$ and 5.

frequency ($\sigma_{AH}$) observed in the IR spectrum. The adjacent Si–H–Si bridges observed in $Si_nH_{4n-1}^+$ form an interesting inorganic hydride wire of the type H–(Si–H)$_n$ in which the H atoms carry negative partial charges. A systematic characterization of individual Si–H–Si bridges as a function of the two Si–H bond lengths ($R_1$ and $R_2$) has been presented in our previous study of $Si_nH_{4n-4}^+$.[33] In general, the more symmetric the Si–H–Si geometry, the stronger the 3c–2e bond. This can be observed in the H–(Si–H)$_n$ wires with $n = 2$ and 4, in which the (inner) 3c–2e bond is rather strong and short with $R_1 = R_2 =$ 1.625 and 1.642 Å, respectively, and $D_0(n = 2) = 150$ kJ mol$^{-1}$. On the other hand, the (outer) 3c–2e bonds for $n = 3$ and 4 are more asymmetric ($R_1 = 1.552/1.519$ Å and $R_2 = 1.809/2.069$ Å), reducing the bond strength to $D_0(n = 3/4) = 41/15$ kJ mol$^{-1}$, respectively. The correlation of the Si–H–Si bond angle with the 3c–2e bond strength is less strong, although it appears that they are more linear for weaker bonds. The observed trend is fully consistent with the analysis of Wiberg bond indices for the two bonds in the Si–H–Si bridge, yielding 0.44/0.44 for $n = 2$, 0.60/0.27 for $n = 3$, and 0.43/0.43 and 0.75/0.14 for the inner and outer bridges of $n = 4$. Clearly, for the weakly-bonded $SiH_4$ ligand in $n =$ 5, the indices of 0.92/0.00 illustrate the situation of a bare van der Waals bond. In general, the H atoms in the 3c–2e bridges carry a substantially more negative partial charge ($q_H = -290$ to $-320$ me) than the free H atoms ($-90$ to $-135$ me). At the same time, the Si atoms carry nearly a full positive charge ($q_{Si} = +800$ to $+960$ me), justifying the view of a hydride bride in the limit of ionic bonding (*e.g.*, $Si^+H^-Si^+$).

In the following, we briefly compare the properties of the $Si_nH_{4n-1}^+$ hydride wires to those of related systems. Overall, due to higher symmetry and the lack of any Si–Si/Si=Si bonds, the IRPD spectra of $Si_nH_{4n-1}^+$ are much simpler and feature less bands than those of the previously studied $Si_nH_{4n-4}^+$ ions,[33] which cannot form a regular hydride wire and lack supersaturation. The bonding of rare gas (Rg) atoms and $H_2$ ligands to the $SiH_3^+$ cation is much weaker than that of $SiH_4$ ligands. Thus, while in $SiH_3^+Rg_{1-2}$ and $SiH_3^+(H_2)_{1-2}$ the ligands form weak van der Waals bonds to the $3p_z$ orbital of $SiH_3^+$,[15,45,46,57] $SiH_4$ ligands form stronger covalent 3c–2e bonds in the $SiH_3^+(SiH_4)_{1-2}$ hydride wires. The interaction of Rg atoms and $H_2$ with the related carbon analogue $CH_3^+$ is much stronger than with $SiH_3^+$, leading to covalent bonds in $CH_3^+Rg$ dimers with heavy Rg atoms and in $CH_5^+$.[51,58–61] As (i) the EN of C is higher than that of H and (ii) C does not like to be penta-coordinated, the $C_nH_{4n-1}^+$ ions do not form supersaturated hydride wires but instead form weakly-bonded van der Waals clusters of $CH_4$ ligands with a covalently-bonded $C_2H_7^+$ core (Fig. S8–S10 in ESI†).[62,63] The linear H–(Si–H)$_n$ hydride wires in $Si_nH_{4n-1}^+$ differ in several aspects from the corresponding proton wires and networks frequently observed, for example in protonated water and ammonia clusters.[64–67] First, the H atoms in $Si_nH_{4n-1}^+$ are negatively charged because EN(Si) < EN(H), while the H atoms in O–H–O and N–H–N bridges are positive because EN(O/N) > EN(H). Moreover, the H–(Si–H)$_n$ hydride wires are essentially one-dimensional (1D), while $H^+(H_2O)_n$ and $H^+(NH_3)_n$ form 2D to 3D networks exhibiting proton transport *via* the Grotthuss mechanism.[68–70] Linear proton wires can be formed for example in protonated imidazole clusters, in which however a heterocyclic spacer is involved.[71–73]

## Conclusions

The interpretation of IRPD spectra of $Si_nH_{4n-1}^+$ ions with $n$ = 2–8 by complementary quantum chemical calculations reveals the formation of an inorganic H–(Si–H)$_n$ hydride wire in the size range $n$ = 2–4, with up three adjacent nonlinear covalent 3c–2e bonds involving penta-coordinated Si atoms. The binding energy with respect to $SiH_4$ elimination becomes weaker as the chain length ($n$) increases. As a result, starting from $n$ = 5 further $SiH_4$ ligands bind weakly to the side of the linear $Si_4H_{15}^+$ chain by induction and dispersion forces. The formation of such a wire is not favourable for the carbon analogue because penta-coordination is highly unfavourable and the EN order (Si < H < C), as illustrated by a comparison of the most stable structures of $C_nH_{4n-1}^+$ and $Si_nH_{4n-1}^+$ (Fig. S8–S9 in ESI†). As a result, the $Si_nH_{4n-1}^+$ clusters are considered to be supersaturated with hydrogen when compared to carbon analogues. The adjacent 3c–2e bonds are associated with the lowest-lying valence MOs, due to their complete delocalization over the whole wire. Due to the relative EN values of Si and H, the $Si_nH_{4n-1}^+$ hydride wires with negatively charged H atoms represent prototypical cationic examples for charge-inverted H-bonds (CIHB)[31–33,41] not yet covered by the IUPAC definition of H-bonds,[43] which thus should be revised for this aspect.[42] Similar to $SiH_3^+$ and $Si_2H_7^+$, longer $Si_nH_{4n-1}^+$ wires may be synthesized and stabilized in the condensed phase. Moreover, such $Si_nH_{4n-1}^+$ ions may be observed in the future in $SiH_4$-rich interstellar regions. Finally, it may be interesting to investigate the effects of substitution of H atoms by functional groups on the properties of such hydride wires.

## Conflicts of interest

There are no conflicts to declare.

## Acknowledgements

This work was supported by Deutsche Forschungsgemeinschaft (project DO 729/9). The authors thank J. Langer, A. Lagutschenkov, and M. Savoca for support in the acquisition of the experimental data.

## References

1 R. D. Miller and J. Michl, *Chem. Rev.*, 1989, **89**, 1359–1410.
2 V. Chandrasekhar, R. Boomishankar and S. Nagendran, *Chem. Rev.*, 2004, **104**, 5847–5910.
3 P. D. Lickiss, in *Adv. Inorg. Chem.*, ed. A. G. Sykes, Academic Press, 1995, vol. 42, pp. 147–262.
4 J. Fischer, J. Baumgartner and C. Marschner, *Science*, 2005, **310**, 825.
5 V. Kumar and Y. Kawazoe, *Phys. Rev. Lett.*, 2003, **90**, 055502.
6 F. Pichierri, V. Kumar and Y. Kawazoe, *Chem. Phys. Lett.*, 2004, **383**, 544–548.
7 R. Singh, *J. Phys.: Condens. Matter*, 2008, **20**, 045226.
8 J. B. Lambert, L. Kania and S. Z. Zhang, *Chem. Rev.*, 1995, **95**, 1191–1201.
9 K. C. Kim, C. A. Reed, D. W. Elliott, L. J. Mueller, F. Tham, L. J. Lin and J. B. Lambert, *Science*, 2002, **297**, 825–827.
10 H. F. T. Klare and M. Oestreich, *Dalton Trans.*, 2010, **39**, 9176–9184.
11 H. F. T. Klare, L. Albers, L. Süsse, S. Keess, T. Müller and M. Oestreich, *Chem. Rev.*, 2021, **121**, 5898–5985.
12 V. Y. Lee, *Russ. Chem. Rev.*, 2019, **88**, 351–369.
13 J. C. L. Walker, H. F. T. Klare and M. Oestreich, *Nat. Rev. Chem.*, 2020, **4**, 54–62.
14 Q. Wu, E. Irran, R. Müller, M. Kaupp, H. F. T. Klare and M. Oestreich, *Science*, 2019, **365**, 168.
15 K. Hiraoka, J. Katsuragawa and A. Minamitsu, *Chem. Phys. Lett.*, 1997, **267**, 580.
16 T. P. Martin and H. Schaber, *J. Chem. Phys.*, 1985, **83**, 855–858.
17 H. Chatham and A. Gallagher, *J. Appl. Phys.*, 1985, **58**, 159–169.
18 M. L. Mandich and W. D. Reents, *J. Chem. Phys.*, 1989, **90**, 3121–3135.
19 M. J. Kushner, *J. Appl. Phys.*, 1993, **74**, 6538–6553.

 

20 G. Turban, Y. Catherine and B. Grolleau, *Plasma Chem. Plasma Process.*, 1982, **2**, 61–80.
21 G. M. Wyller, T. J. Preston, H. Klette, T. Mongstad and E. S. Marstein, *J. Cryst. Growth*, 2018, **498**, 315–327.
22 D. M. Goldhaber and A. L. Betz, *Astrophys. J.*, 1984, **279**, L55–L58.
23 B. A. McGuire, *Astrophys. J., Suppl. Ser.*, 2022, **259**, 30.
24 M. C. McCarthy, C. A. Gottlieb and P. Thaddeus, *Mol. Phys.*, 2003, **101**, 697–704.
25 E. Herbst, T. J. Millar, S. Wlodek and D. K. Bohme, *Astron. Astrophys.*, 1989, **222**, 205–210.
26 F. Fang, Q. Jiang and R. S. Klausen, *J. Am. Chem. Soc.*, 2022, **144**, 7834–7843.
27 G. Tarczay, M. Förstel, P. Maksyutenko and R. I. Kaiser, *Inorg. Chem.*, 2016, **55**, 8776–8785.
28 N. Goldberg and H. Schwarz, in *The Chemistry of Organic Silicon Compounds*, ed. Z. Rappoport and Y. Apeloig, Wiley, 1998, ch. 18, vol. 2, pp. 1105–1142.
29 S. Fornarini, *The Chemistry of Organic Silicon Compounds*, 2001, ch. 18, pp. 1027–1057.
30 M. Savoca, M. A. R. George, J. Langer and O. Dopfer, *Phys. Chem. Chem. Phys.*, 2013, **15**, 2774–2781.
31 M. Savoca, J. Langer and O. Dopfer, *Angew. Chem., Int. Ed.*, 2013, **52**, 1568–1571.
32 M. A. R. George, M. Savoca and O. Dopfer, *Chem. – Eur. J.*, 2013, **19**, 15315–15328.
33 M. A. R. George and O. Dopfer, *Int. J. Mass Spectrom.*, 2019, **435**, 51–60.
34 S. Patai and Z. Rappoport, *The Chemistry of Organic Silicon Compounds*, Wiley, Chichester, 1989.
35 R. L. DeKock and W. B. Bosma, *J. Chem. Educ.*, 1988, **65**, 194–197.
36 J. E. McMurry and T. Lectka, *Acc. Chem. Res.*, 1992, **25**, 47–53.
37 S. K. Estreicher, *Mater. Sci. Eng., R*, 1995, **14**, 319–412.
38 T. Müller, *Angew. Chem., Int. Ed.*, 2001, **40**, 3033–3036.
39 R. Panisch, M. Bolte and T. Müller, *J. Am. Chem. Soc.*, 2006, **128**, 9676–9682.
40 S. P. Hoffmann, T. Kato, F. S. Tham and C. A. Reed, *Chem. Commun.*, 2006, 767–769.
41 M. Jablonski, *Chem. Phys. Lett.*, 2009, **477**, 374–376.
42 S. Civiš, M. Lamanec, V. Špirko, J. Kubišta, M. Špet'ko and P. Hobza, *J. Am. Chem. Soc.*, 2023, **145**, 8550–8559.
43 E. Arunan, G. R. Desiraju, R. A. Klein, J. Sadlej, S. Scheiner, I. Alkorta, D. C. Clary, R. H. Crabtree, J. J. Dannenberg, P. Hobza, H. G. Kjaergaard, A. C. Legon, B. Mennucci and D. J. Nesbitt, *Pure Appl. Chem.*, 2011, **83**, 1637–1641.
44 D. M. Smith, P. M. Martineau and P. B. Davies, *J. Chem. Phys.*, 1992, **96**, 1741.
45 Y. B. Cao, J. H. Choi, B. M. Haas, M. S. Johnson and M. Okumura, *J. Phys. Chem.*, 1993, **97**, 5215–5217.
46 D. W. Boo and Y. T. Lee, *J. Chem. Phys.*, 1995, **103**, 514–519.
47 T. Y. Yu, T. M. H. Cheng, F. W. Lampe and V. Kempter, *J. Phys. Chem.*, 1972, **76**, 3321–3330.
48 A. Ding, R. A. Cassidy, L. S. Cordis and F. W. Lampe, *J. Chem. Phys.*, 1985, **83**, 3426–3432.
49 K. Raghavachari, *J. Chem. Phys.*, 1990, **92**, 452–465.
50 L. A. Curtiss, K. Raghavachari, P. W. Deutsch and J. A. Pople, *J. Chem. Phys.*, 1991, **95**, 2433–2444.
51 O. Dopfer, *Int. Rev. Phys. Chem.*, 2003, **22**, 437–495.
52 O. Dopfer, *Z. Phys. Chem.*, 2005, **219**, 125–168.
53 M. A. R. George, N. X. Truong, M. Savoca and O. Dopfer, *Angew. Chem., Int. Ed.*, 2018, **57**, 2919–2923.
54 T. Shimanouchi, *Tables of Molecular Vibrational Frequencies, Consolidated Volume I*, NSRDS-NBS, 1972.
55 P. Botschwina and M. Oswald, *J. Chem. Phys.*, 1992, **96**, 4044–4045.
56 J. Kapp, P. R. Schreiner and P. v R. Schleyer, *J. Am. Chem. Soc.*, 1996, **118**, 12154–12158.
57 S. Pan, D. Moreno, G. Merino and P. Chattaraj, *Chem. Phys. Chem.*, 2014, **15**, 3554–3564.
58 R. V. Olkhov, S. A. Nizkorodov and O. Dopfer, *J. Chem. Phys.*, 1998, **108**, 10046–10060.
59 D. W. Boo, Z. F. Liu, A. G. Suits, J. S. Tse and Y. T. Lee, *Science*, 1995, **269**, 57–59.
60 S. P. Gnanasekar and E. Arunan, *J. Phys. Chem. A*, 2019, **123**, 1168–1176.
61 O. Asvany, K. M. T. Yamada, S. Brunken, A. Potapov and S. Schlemmer, *Science*, 2015, **347**, 1346–1349.
62 K. Hiraoka and P. Kebarle, *J. Am. Chem. Soc.*, 1976, **98**, 6119–6125.
63 L. I. Yeh, J. M. Price and Y. T. Lee, *J. Am. Chem. Soc.*, 1989, **111**, 5597.
64 M. Miyazaki, A. Fujii, T. Ebata and N. Mikami, *Science*, 2004, **304**, 1134–1137.
65 J.-W. Shin, N. I. Hammer, E. G. Diken, M. A. Johnson, R. S. Walters, T. D. Jaeger, M. A. Duncan, R. A. Christie and K. D. Jordan, *Science*, 2004, **304**, 1137–1140.
66 M. Park, I. Shin, N. J. Singh and K. S. Kim, *J. Phys. Chem.*, 2007, **111**, 10692–10702.
67 M. Katada, R. Shishido and A. Fujii, *Phys. Chem. Chem. Phys.*, 2014, **16**, 7595–7601.
68 C. J. D. Grotthuss, *Ann. Chim. Phys.*, 1806, **58**, 54–57.
69 N. Agmon, *Chem. Phys. Lett.*, 1995, **244**, 456.
70 D. Marx, *Chem. Phys. Chem.*, 2006, **7**, 1848–1870.
71 W. Münch, K. D. Kreuer, W. Silvestri, J. Maier and G. Seifert, *Solid State Ionics*, 2001, **145**, 437–443.
72 H. K. Gerardi, G. H. Gardenier, U. Viswanathan, S. M. Auerbach and M. A. Johnson, *Chem. Phys. Lett.*, 2011, **501**, 172–178.
73 A. A. Adesokan, G. M. Chaban, O. Dopfer and R. B. Gerber, *J. Phys. Chem. A*, 2007, **111**, 7374–7381.